

Understanding Sources of Demographic Predictability in Brain MRI via Disentangling Anatomy and Contrast

Mehmet Yigit Avci^{*1}, Akshit Achara^{*1}, Andrew King^{†1}, Jorge Cardoso^{†1}, and
for the Alzheimer’s Disease Neuroimaging Initiative

School of Biomedical Engineering & Imaging Sciences, King’s College London,
London, UK

Abstract. Demographic attributes such as age, sex, and race can be predicted from medical images, raising concerns about bias in clinical AI systems. In brain MRI, this signal may arise from anatomical variation, acquisition-dependent contrast differences, or both, yet these sources remain entangled in conventional analyses. Without disentangling them, mitigation strategies risk failing to address the underlying causes. We propose a controlled framework based on disentangled representation learning, decomposing brain MRI into anatomy-focused representations that suppress acquisition influence and contrast embeddings that capture acquisition-dependent characteristics. Training predictive models for age, sex, and race on full images, anatomical representations, and contrast-only embeddings allows us to quantify the relative contributions of structure and acquisition to the demographic signal. Across three datasets and multiple MRI sequences, we find that demographic predictability is primarily rooted in anatomical variation: anatomy-focused representations largely preserve the performance of models trained on raw images. Contrast-only embeddings retain a weaker but systematic signal that is dataset-specific and does not generalise across sites. These findings suggest that effective mitigation must explicitly account for the distinct anatomical and acquisition-dependent origins of the demographic signal, ensuring that any bias reduction generalizes robustly across domains.

Keywords: Fairness · Bias · Disentanglement · Representation Learning

1 Introduction

Medical imaging plays a central role in modern clinical practice and biomedical research, supporting diagnosis, treatment planning, and disease monitoring across a wide range of modalities. Advances in machine learning have enabled models that extract rich information from medical images for tasks such as segmentation, classification, and prognosis. However, growing evidence suggests

^{*} These authors contributed equally to this work.

[†] These authors jointly supervised this work.

that machine learning models may encode and exploit unintended correlations present in imaging data, leading to systematic performance disparities across demographic groups, with attributes such as race remaining identifiable even when clinically unrelated to the target task [22,14,25,19,7,19]. Attempts to mitigate these effects through generic fairness interventions have proven insufficient, often degrading performance or failing under real-world distribution shifts [21]. These observations suggest that the demographic signal is not a superficial modelling artifact but reflects structured variation embedded within the data itself.

Recent work has begun to investigate where this signal originates. For example, in cardiac MRI segmentation, demographic information has been shown to persist within learned representations despite controlled task settings [15]. In chest X-ray classification, acquisition-related factors substantially contribute to the demographic signal and downstream performance disparities [16]. Collectively, these findings indicate that bias may emerge not only from population imbalance, but also from modality- and acquisition-specific characteristics that models implicitly exploit.

This perspective is particularly relevant for brain MRI. Although demographic bias has been documented in MRI-based models [1,18,6], its origins remain unclear. Brain MRI is intrinsically heterogeneous: image appearance is governed by interactions between sequence parameters (e.g., TR, TE), scanner hardware, and site-specific protocols. These acquisition-dependent factors systematically shape intensity distributions and tissue contrast, introducing variability sources that correlate with demographic attributes. As anatomical structure and acquisition-dependent contrast are entangled in raw images, conventional models cannot determine whether the demographic signal arises from biological variation, acquisition settings, or their interaction.

To understand the underlying drivers of demographic bias in brain MRI, we employ disentangled representation learning frameworks, specifically MR-CLIP [4] and DIST-CLIP [3]. These models decompose brain MRI into distinct anatomical images and contrast-only embeddings, enabling explicit separation of structural information from acquisition-dependent signal. We train predictive models for age, sex, and race using (i) full brain MRI images, (ii) anatomy-focused images that are independent of contrast, and (iii) contrast-only embeddings that capture acquisition characteristics while minimizing anatomical content. By comparing predictive performance across these representations, we quantify the relative contributions of anatomical structure and acquisition-induced contrast to the demographic signal. Our contributions are: (1) a controlled framework for disentangling anatomical and acquisition-dependent sources of the demographic signal in brain MRI; (2) evidence, across three datasets and multiple MRI sequences, that anatomical structure is the dominant carrier of demographic information; and (3) showing that contrast-only embeddings retain a weaker, dataset-specific signal that does not generalise across sites, establishing that effective bias mitigation strategies must address both sources.

2 Methods

2.1 Experimental Design

Let $\mathcal{D} = \{(x_i, y_i, a_i)\}_{i=1}^N$ denote a dataset of brain MRI scans $x_i \in \mathcal{X}$, demographic attributes $y_i \in \mathcal{Y}$ (age, sex, race), and acquisition metadata $a_i \in \mathcal{A}$ (e.g., TR, TE, scanner type, site). Our objective is to determine whether the demographic signal arises primarily from anatomical structure, acquisition-dependent contrast, or their interaction.

In raw MRI, anatomical structure and contrast are inherently entangled within the image space \mathcal{X} . We therefore seek a representation-level decomposition of each image x into two components,

$$x \longrightarrow (z_{\text{anat}}, z_{\text{contrast}}), \quad (1)$$

where $z_{\text{anat}} \in \mathcal{Z}_{\text{anat}}$ captures structural information while minimizing acquisition effects, and $z_{\text{contrast}} \in \mathcal{Z}_{\text{contrast}}$ captures acquisition-dependent signal while reducing anatomical dominance. To operationalize this separation, we leverage pre-trained disentangled representation learning frameworks, MR-CLIP [4] and DIST-CLIP [3]. MR-CLIP is a metadata-guided contrastive learning framework that aligns MRI images with their associated DICOM acquisition parameters without requiring manual sequence labels. An image encoder E_I and a metadata encoder E_M are trained jointly so that the image embedding $z_{\text{contrast}}^x = E_I(x)$ and the metadata embedding $z^a = E_M(a)$ are similar for matched pairs and dissimilar for mismatches. By optimizing a contrastive objective over image-metadata pairs drawn from diverse scanners and parameter settings, MR-CLIP learns a 512-dimensional embedding that reflects systematic contrast variations induced by acquisition differences [2,4]. DIST-CLIP builds upon MR-CLIP by introducing an explicit anatomical pathway to separate structural content from acquisition-dependent contrast. It employs an anatomy mapper that projects an input image x to an anatomy-focused representation z_{anat} . This representation is designed to preserve geometric and morphological structure while suppressing intensity and contrast-related cues. To enforce acquisition invariance, DIST-CLIP incorporates contrastive loss applied at the patch level across anatomy images. This loss encourages corresponding anatomical patches from images acquired with different protocols to remain similar in the z_{anat} space, regardless of acquisition differences. This explicitly promotes structural consistency while discouraging the encoding of contrast-specific information. As a result, the model achieves a disentangled decomposition in which z_{anat} captures acquisition-invariant information, while z_{contrast} encodes acquisition-dependent characteristics [3].

Fig. 1 illustrates the proposed disentanglement qualitatively and quantitatively. Panel A shows representative raw T1-weighted images from OASIS, HCP, and ADNI alongside their corresponding anatomical images (z_{anat}). While the raw images reflect both structural content and site-specific contrast differences, the anatomy-focused representations preserve geometric structure while suppressing acquisition-driven intensity variations. Panel B visualizes contrast-only

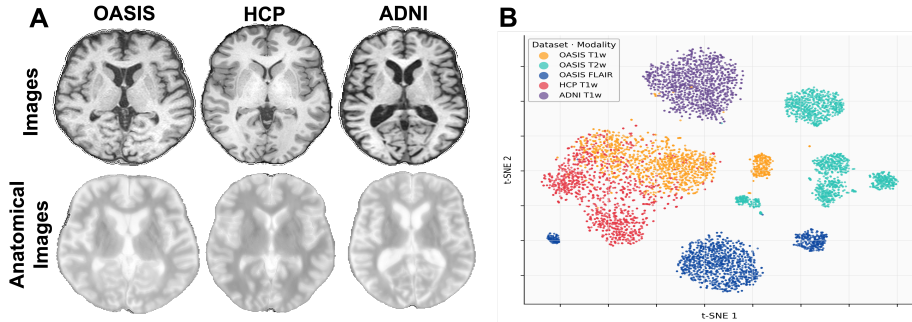


Fig. 1. Qualitative and embedding-level visualization of the disentanglement. **A:** Raw images (x , top) and anatomy-focused representations (z_{anat} , bottom). **B:** t-SNE of contrast embeddings (z_{contrast}) showing acquisition-driven clustering.

embeddings (z_{contrast}) using t-SNE. The clear clustering by dataset and sequence (e.g., T1w, T2w, FLAIR) indicates that these embeddings capture acquisition-dependent characteristics.

To quantify the contribution of each representation to the demographic signal, we define three predictive mappings:

$$\begin{aligned} f_{\text{full}} &: \mathcal{X} \rightarrow \mathcal{Y}, \\ f_{\text{anat}} &: \mathcal{Z}_{\text{anat}} \rightarrow \mathcal{Y}, \\ f_{\text{contrast}} &: \mathcal{Z}_{\text{contrast}} \rightarrow \mathcal{Y}. \end{aligned}$$

Here, f_{full} is trained directly on raw MRI x , while f_{anat} and f_{contrast} operate on disentangled representations z_{anat} and z_{contrast} , respectively. For each demographic attribute $y \in \{\text{age, sex, race}\}$, we train models under identical optimization protocols and compare predictive performance across these mappings. Performance differences between f_{anat} and f_{contrast} provide an empirical estimate of the relative contribution of anatomical structure and acquisition-dependent contrast to the demographic signal. The performance of f_{full} serves as a reference for the total demographic information accessible from the raw image x .

2.2 Models and Evaluation

For image-based inputs (f_{full} and f_{anat}), we employ a 3D ResNet-50 architecture [9,23] operating on volumetric inputs of size $128 \times 128 \times 128$. All models are initialized from ImageNet-pretrained weights (inflated to 3D). A fixed learning rate of 1×10^{-4} is used across all experiments with dropout regularization of 0.2 to mitigate overfitting. The batch size is 2 due to memory constraints of 3D training. For embedding-based inputs (f_{contrast}), we use a multi-layer perceptron operating on z_{contrast} with architecture $512 \text{ (input)} \rightarrow 512 \rightarrow 256 \rightarrow N_{\text{classes}}$, with ReLU activations and dropout (0.2) applied after each hidden layer.

Age prediction is formulated as a regression task optimized using mean squared error (MSE) (HCP age uses range midpoint). Sex and race prediction are formulated as classification tasks optimized with cross-entropy loss. All models are trained under matched data splits, learning rates, and regularization schemes to ensure comparability across representation types. We report mean absolute error (MAE) for age prediction and balanced accuracy (BalAcc) for classification tasks, ensuring equal weighting of classes to account for potential imbalance. Balanced accuracy is defined as the average recall across classes (i.e., mean per-class sensitivity), thereby preventing inflated performance estimates in the presence of class imbalance.

2.3 Datasets and Preprocessing

We evaluate our approach on three publicly available brain MRI datasets: Open Access Series of Imaging Studies (OASIS) [13], Alzheimer’s Disease Neuroimaging Initiative (ADNI) [11], and Human Connectome Project (HCP) [24]. These cohorts span different age ranges, scanner vendors, and acquisition protocols, providing diverse combinations of (x_i, a_i, y_i) for analyzing acquisition-driven effects on demographic predictability. This heterogeneity is essential for disentangling anatomical structure from contrast variations induced by imaging parameters. The demographic distribution of each dataset, including age, sex, and race, is summarized in Table 1. To ensure consistency across datasets and compatibility with the disentanglement framework, all volumes are rigidly registered to the MNI152 atlas at 1.0mm^3 isotropic resolution. Skull stripping is performed using SynthStrip [10].

Table 1. Subject-level demographic summary of the included datasets. Age is reported as mean \pm standard deviation. Sex and race are reported as counts (percentage within dataset).

Dataset	Age	Sex		Race	
	Mean \pm SD	Female	Male	White	Black
OASIS-3	72.4 \pm 9.1	608 (55.6%)	485 (44.4%)	926 (84.7%)	167 (15.3%)
ADNI	74.7 \pm 7.3	725 (44.6%)	901 (55.4%)	1542 (94.8%)	84 (5.2%)
HCP	29.1 \pm 3.5	543 (54.4%)	455 (45.6%)	830 (83.2%)	168 (16.8%)

3 Experiments and Results

We first evaluate the demographic signal within each dataset using T1-weighted images under matched train–test conditions to quantify the relative contributions of structural (z_{anat}) and acquisition-dependent (z_{contrast}) representations

(Table 2). Models trained on raw images achieve the highest overall performance across tasks (e.g., sex BalAcc 0.92–0.96; race BalAcc 0.86–0.97; age MAE 2.67–5.15 years). Anatomy-focused representations largely preserve this performance, for instance, sex prediction reaches 0.93 in OASIS and 0.96 in HCP, indicating that substantial demographic signal is embedded in structural variation. When training jointly across all datasets, this pattern remains consistent (Sex 0.96 Raw vs. 0.96 Anat vs. 0.78 Contrast), suggesting that the dominance of anatomical signal is not driven by single-dataset effects. Importantly, contrast-only embeddings—despite explicitly minimizing anatomical content—retain non-trivial predictive power. Sex prediction from z_{contrast} achieves BalAcc 0.71 in OASIS and 0.81 in HCP (0.78 in joint training), while race prediction remains above chance in OASIS (0.71), HCP (0.70), and joint training (0.68). Even for age, contrast embeddings yield informative MAE values (e.g., 6.28 years in OASIS, 2.77 years in HCP, and 5.21 jointly). Although consistently lower than raw and anatomy-based models, these results demonstrate that acquisition-dependent contrast alone carries a measurable demographic signal.

Table 2. Within-dataset and joint-training performance across representations. For each dataset (OASIS, ADNI, HCP) and joint training across all datasets (ALL), we report balanced accuracy (BalAcc, \uparrow ; equal class weighting) for **Sex** and **Race**, and mean absolute error (MAE, \downarrow) for **Age**.

Dataset	Sex (BalAcc \uparrow)			Race (BalAcc \uparrow)			Age (MAE \downarrow)		
	Raw	Anat	Contrast	Raw	Anat	Contrast	Raw	Anat	Contrast
OASIS	0.92	0.93	0.71	0.86	0.81	0.71	5.15	5.45	6.28
ADNI	0.94	0.93	0.74	0.97	0.82	0.50	4.46	4.43	5.61
HCP	0.95	0.96	0.81	0.96	0.90	0.70	2.67	2.99	2.77
ALL	0.96	0.96	0.78	0.91	0.93	0.68	3.91	4.35	5.21

To further investigate whether demographic signal reflects stable biological variation or dataset-specific acquisition effects, we evaluate cross-dataset generalization. We train models on one dataset and test on another, thereby introducing a shift in acquisition protocols, scanner vendors, and population characteristics. This setting allows us to assess whether the demographic signal persists when acquisition-dependent correlations no longer match between training and testing distributions (Table 3).

Across all tasks, performance drops markedly under dataset shift, particularly for age prediction, where MAE increases dramatically (e.g., HCP→ADNI: Raw 42.39 years). For classification, a consistent pattern emerges: anatomy-focused representations (z_{anat}) tend to generalize more robustly than raw images. For example, OASIS→HCP sex prediction improves from BalAcc 0.65 (Raw) to 0.82 (Anat), and ADNI→HCP improves from 0.63 to 0.82. Whereas, contrast-only embeddings (z_{contrast}) frequently collapse toward chance (0.50), indicating

Table 3. Cross-dataset generalization. **Sex** and **Race** are reported as balanced accuracy (BalAcc, \uparrow ; equal class weighting), and **Age** is reported as mean absolute error (MAE, \downarrow).

Train	Test	Sex (BalAcc \uparrow)			Race (BalAcc \uparrow)			Age (MAE \downarrow)		
		Raw	Anat	Contrast	Raw	Anat	Contrast	Raw	Anat	Contrast
OASIS	HCP	0.65	0.82	0.50	0.85	0.87	0.50	26.37	28.03	29.89
	ADNI	0.88	0.89	0.59	0.93	0.99	0.53	5.15	5.50	8.71
HCP	OASIS	0.72	0.71	0.53	0.85	0.82	0.70	39.55	42.42	46.91
	ADNI	0.60	0.61	0.50	0.88	0.84	0.60	42.39	44.24	50.61
ADNI	OASIS	0.76	0.84	0.70	0.81	0.84	0.50	5.17	5.49	6.47
	HCP	0.62	0.81	0.51	0.86	0.90	0.50	29.58	28.11	30.77

poor transferability of acquisition-dependent signal. These findings suggest that while contrast embeddings encode measurable demographic information within a dataset, much of this signal is dataset-specific and does not generalize across sites. Structural representations, in contrast, retain more stable demographic information under distribution shift. Together with the within-dataset results, this indicates that demographic predictability in brain MRI arises from both anatomical and acquisition-related sources, but acquisition-driven correlations are less robust and more site-dependent.

We further investigate the demographic signal across imaging sequences within OASIS (Table 4) to assess whether the relative roles of anatomy and contrast vary with sequence type. Across T2w and FLAIR images, anatomy-focused representations remain close to raw performance (e.g., sex BalAcc 0.91 vs. 0.90 for T2w), indicating that structural variation continues to account for a substantial portion of the demographic signal beyond T1-weighted imaging. Importantly, contrast-only embeddings retain measurable predictive power across sequences. For example, sex prediction from z_{contrast} reaches BalAcc 0.72 in T2w and 0.75 in FLAIR. However, race prediction remains near chance in T2w and FLAIR. Joint training on all sequences maintains strong sex prediction performance (BalAcc 0.91), suggesting that combining contrasts does not remove demographic signal.

Table 4. OASIS multi-sequence analysis. Performance across sequences for models trained on raw images (f_{full}), anatomy-focused representations (f_{anat}), and contrast-only embeddings (f_{contrast}). **Sex** and **Race** are reported as balanced accuracy (BalAcc, \uparrow ; equal class weighting). **Age** is reported as mean absolute error (MAE, \downarrow).

Sequence	Sex (BalAcc \uparrow)			Race (BalAcc \uparrow)			Age (MAE \downarrow)		
	Raw	Anat	Contrast	Raw	Anat	Contrast	Raw	Anat	Contrast
T1w	0.92	0.93	0.71	0.86	0.81	0.71	5.15	5.45	6.28
T2w	0.91	0.90	0.72	0.74	0.88	0.51	5.44	5.91	6.60
FLAIR	0.71	0.83	0.75	0.65	0.85	0.50	4.54	4.80	6.67
All Sequences	0.91	0.93	0.76	0.84	0.81	0.70	5.37	5.16	5.90

Anatomy-focused representations continue to perform strongly (sex BalAcc 0.93, race BalAcc 0.81, age MAE 5.16), while contrast embeddings remain weaker yet informative. Overall, the consistency of these trends across sequences indicates that the demographic signal is not specific to a single modality, but reflects contributions from both anatomical structure and acquisition-related contrast properties.

4 Discussion

In this study, we go beyond showing that demographic attributes can be predicted from brain MRI to address a more fundamental question: where does this signal originate? By explicitly decomposing MRI into anatomy-focused and contrast-dependent representations, we provide a principled framework that allows the demographic signal to be attributed to distinct sources, enabling mechanistic insights rather than mere quantification of its presence.

Our results consistently show that the majority of the demographic signal is preserved in anatomy-focused representations, establishing structural variation as the dominant contributor. This aligns with biological expectations for age and is plausible for sex, given known morphological differences [17,8,20], and there is evidence that relative brain volume can differ across racial and ethnic groups [5,12]. At the same time, contrast-only embeddings retain stable, above-chance predictive performance across datasets and sequences. Although weaker than anatomy-based models, this effect is systematic and reproducible, suggesting that acquisition characteristics form structured patterns that correlate with demographic distributions.

These findings carry important implications. Because a substantial portion of the demographic signal resides in anatomical structure, approaches that focus exclusively on acquisition harmonization or intensity normalization may not fully address demographic predictability in downstream applications such as Alzheimer’s disease detection. At the same time, strategies that indiscriminately suppress anatomical variation could inadvertently affect clinically meaningful information. Therefore, effective mitigation strategies should explicitly account for both anatomical and acquisition-dependent sources of demographic signal, for example by combining representation-level debiasing with careful evaluation of how each source influences specific clinical tasks, ensuring that bias reduction generalizes across domains.

A limitation of this study is the imbalanced racial composition of the included datasets, particularly ADNI, where only 84 participants (5.2%) are Black. Although balanced accuracy mitigates the effect of class imbalance on the reported metrics, the small minority-class size limits the statistical reliability of race prediction results. Future work should evaluate these effects in more demographically representative cohorts.

Identifying demographic signal does not in itself imply harmful bias in clinical predictions. However, understanding where this signal resides is a prerequisite for evaluating its downstream impact. Our framework provides a basis for in-

vestigating how these components propagate into clinical tasks and under what conditions they may translate into measurable bias, supporting the development of causally informed and fair neuroimaging models.

Acknowledgments. This research was supported by the UK Engineering and Physical Sciences Research Council (EPSRC) [Grant reference number EP/Y035216/1] Centre for Doctoral Training in Data-Driven Health (DRIVE-Health) at King’s College London with additional support from deepc GMBH. Further support is given by Scientific and Technological Research Council of Türkiye (TÜBİTAK) under 2213-A Overseas Graduate Scholarship. Data used in preparation of this article were obtained from the Alzheimer’s Disease Neuroimaging Initiative (ADNI) database (adni.loni.usc.edu). As such, the investigators within the ADNI contributed to the design and implementation of ADNI and/or provided data but did not participate in analysis or writing of this report. A complete listing of ADNI investigators can be found at: <http://adni.loni.usc.edu/wp-content/uploads/howtoapply/ADNIAcknowledgementList.pdf>. Data were also provided in part by OASIS and the Human Connectome Project, WU-Minn Consortium (Principal Investigators: David Van Essen and Kamil Ugurbil; 1U54MH091657) funded by the 16 NIH Institutes and Centers that support the NIH Blueprint for Neuroscience Research; and by the McDonnell Center for Systems Neuroscience at Washington University.

Disclosure of Interests. The authors have no competing interests to declare that are relevant to the content of this article.

References

1. Achara, A., Anton, E.P., Hammers, A., King, A.P.: Invisible attributes, visible biases: Exploring demographic shortcuts in mri-based alzheimer’s disease classification (2025), <https://arxiv.org/abs/2509.09558>
2. Avci, M.Y., Borges, P., Wright, P., Yigitsoy, M., Ourselin, S., Cardoso, J.: MR-CLIP: Efficient metadata-guided learning of MRI contrast representations. In: Cui, Z., Reikik, A., Suk, H.I., Ouyang, X., Sun, K., Wang, S. (eds.) Machine Learning in Medical Imaging. MLMI 2025, Lecture Notes in Computer Science, vol. 16241. Springer, Cham (2026)
3. Avci, M.Y., Borges, P., Fernandez, V., Wright, P., Yigitsoy, M., Ourselin, S., Cardoso, J.: DIST-CLIP: Arbitrary metadata and image guided MRI harmonization via disentangled anatomy-contrast representations (2025), <https://arxiv.org/abs/2512.07674>
4. Avci, M.Y., Borges, P., Fernandez, V., Wright, P., Yigitsoy, M., Ourselin, S., Cardoso, J.: Metadata-aligned 3D MRI representations for contrast understanding and quality control. arXiv:2511.00681 (2025)
5. Brickman, A.M., Schupf, N., Manly, J.J., Luchsinger, J.A., Andrews, H., Tang, M.X., Reitz, C., Small, S.A., Mayeux, R., DeCarli, C., Brown, T.R.: Brain morphology in older african americans, caribbean hispanics, and whites from northern manhattan. *Archives of Neurology* **65**(8), 1053–1061 (08 2008)
6. Danaee, G., Niethammer, M., Rushmore, J., Bouix, S.: Investigating demographic bias in brain mri segmentation: A comparative study of deep-learning and non-deep-learning methods. *Machine Learning for Biomedical Imaging* **3**, 792–808 (2025)

7. Gichoya, J.W., Banerjee, I., Bhimireddy, A.R., Burns, J.L., Celi, L.A., Chen, L.C., Correa, R., Dullerud, N., Ghassemi, M., Huang, S.C., Kuo, P.C., Lungren, M.P., Palmer, L.J., Price, B.J., Purkayastha, S., Pyrros, A.T., Oakden-Rayner, L., Okechukwu, C., Seyyed-Kalantari, L., Trivedi, H., Wang, R., Zaiman, Z., Zhang, H.: AI recognition of patient race in medical imaging: a modelling study. *The Lancet Digital Health* **4**(6), e406–e414 (2022)
8. Good, C.D., Johnsrude, I., Ashburner, J., Henson, R.N., Friston, K.J., Frackowiak, R.S.: Cerebral asymmetry and the effects of sex and handedness on brain structure: a voxel-based morphometric analysis of 465 normal adult human brains. *Neuroimage* **14**(3), 685–700 (2001)
9. He, K., Zhang, X., Ren, S., Sun, J.: Deep residual learning for image recognition (2015), <https://arxiv.org/abs/1512.03385>
10. Hoopes, A., Mora, J.S., Dalca, A.V., Fischl, B., Hoffmann, M.: SynthStrip: skull-stripping for any brain image. *NeuroImage* **260**, 119474 (2022)
11. Jack, C.R.J., Bernstein, M.A., Fox, N.C., Thompson, P., Alexander, G., Harvey, D., Borowski, B., Britson, P.J., Whitwell, J.L., Ward, C., Dale, A.M., Felmlee, J.P., Gunter, J.L., Hill, D.L., Killiany, R., Schuff, N., Fox-Bosetti, S., Lin, C.P., Studholme, C., DeCarli, C.S., Krueger, G., Ward, H.A., Metzger, G.J., Scott, K.T., Mallozzi, R., Blezek, D., Levy, J., Debbins, J.P., Fleisher, A.S., Albert, M., Green, R., Bartzokis, G., Glover, G., Mugler, J., Weiner, M.W.: The Alzheimer’s Disease Neuroimaging Initiative (ADNI): MRI methods. *Journal of Magnetic Resonance Imaging* **27**(4), 685–691 (2008)
12. Kang, D.W., Wang, S.M., Na, H.R., Park, S.Y., Kim, N.Y., Lee, C.U., Kim, D., Son, S.J., Lim, H.K.: Differences in cortical structure between cognitively normal east asian and caucasian older adults: a surface-based morphometry study. *Scientific reports* **10**(1), 20905 (2020)
13. LaMontagne, P.J., Benzinger, T.L., Morris, J.C., Keefe, S., Hornbeck, R., Xiong, C., Grant, E., Hassenstab, J., Moulder, K., Vlassenko, A., Raichle, M.E., Cruchaga, C., Marcus, D.: Oasis-3: Longitudinal neuroimaging, clinical, and cognitive dataset for normal aging and alzheimer disease. *medRxiv* (2019)
14. Larrazabal, A.J., Nieto, N., Peterson, V., Milone, D.H., Ferrante, E.: Gender imbalance in medical imaging datasets produces biased classifiers for computer-aided diagnosis. *Proceedings of the National Academy of Sciences* **117**(23), 12592–12594 (2020)
15. Lee, T., Puyol-Anton, E., Ruijsink, B., Masci, P.G., Keehn, L., Chowienczyk, P., Haseler, E., Shi, M., King, A.: Understanding-informed bias mitigation for fair CMR segmentation. *Machine Learning for Biomedical Imaging* **3**(Special on FAIMI), 808–824 (2025)
16. Lotter, W.: Acquisition parameters influence AI recognition of race in chest X-rays and mitigating these factors reduces underdiagnosis bias. *Nature Communications* **15**, 7465 (2024)
17. Passe, T.J., Rajagopalan, P., Tupler, L.A., Byrum, C.E., Macfall, J.R., Krishnan, K.R.: Age and sex effects on brain morphology. *Progress in Neuro-Psychopharmacology and Biological Psychiatry* **21**(8), 1231–1237 (1997)
18. Petersen, E., Feragen, A., da Costa Zemsch, M.L., Henriksen, A., Wiese Christensen, O.E., Ganz, M.: Feature robustness and sex differences in medical imaging: A case study in MRI-based Alzheimer’s Disease detection. In: "Wang, L., Dou, Q., Fletcher, P.T., Speidel, S., Li, S. (eds.) *Medical Image Computing and Computer Assisted Intervention – MICCAI 2022*. pp. 88–98. Springer Nature Switzerland, Cham (2022)

19. Puyol-Antón, E., Ruijsink, B., Piechnik, S.K., Neubauer, S., Petersen, S.E., Razavi, R., King, A.P.: Fairness in cardiac mr image analysis: An investigation of bias due to data imbalance in deep learning based segmentation. In: de Bruijne, M., Cattin, P.C., Cotin, S., Padoy, N., Speidel, S., Zheng, Y., Essert, C. (eds.) *Medical Image Computing and Computer Assisted Intervention – MICCAI 2021*. pp. 413–423. Springer International Publishing, Cham (2021)
20. Ruigrok, A.N., Salimi-Khorshidi, G., Lai, M.C., Baron-Cohen, S., Lombardo, M.V., Tait, R.J., Suckling, J.: A meta-analysis of sex differences in human brain structure. *Neuroscience & Biobehavioral Reviews* **39**, 34–50 (2014)
21. Schrouff, J., Harris, N., Koyejo, O., Alabdulmohsin, I., Schnider, E., Opsahl-Ong, K., Brown, A., Roy, S., Mincú, D., Chen, C., Dieng, A., Liu, Y., Natarajan, V., Karthikesalingam, A., Heller, K., Chiappa, S., D’Amour, A.: Diagnosing failures of fairness transfer across distribution shift in real-world medical settings (2023), <https://arxiv.org/abs/2202.01034>
22. Seyyed-Kalantari, L., Zhang, H., McDermott, M., Chen, I., Marzyeh, G.: Under-diagnosis bias of artificial intelligence algorithms applied to chest radiographs in under-served patient populations. *Nature Medicine* **27**, 2176–2182 (2021)
23. Solovyev, R., Kalinin, A.A., Gabruseva, T.: 3d convolutional neural networks for stalled brain capillary detection. *Computers in Biology and Medicine* **141**, 105089 (2022). <https://doi.org/10.1016/j.combiomed.2021.105089>
24. Van Essen, D.C., Smith, S.M., Barch, D.M., Behrens, T.E., Yacoub, E., Ugurbil, K.: The WU-Minn Human Connectome Project: An overview. *NeuroImage* **80**, 62–79 (2013)
25. Waite, S., Scott, J., Colombo, D.: Narrowing the gap: Imaging disparities in radiology. *Radiology* **299**(1), 27–35 (2021), PMID: 33560191